de Villiers *et al. Earth, Planets and Space* (2016) 68:154
DOI 10.1186/s40623-016-0530-1

Earth, Planets and Space

FULL PAPER

Open Access

Estimating ionospheric currents by inversion from ground-based geomagnetic data and calculating geoelectric fields for studies of geomagnetically induced currents

J. S. de Villiers[1*], R. J. Pirjola[2,3] and P. J. Cilliers[1,4]

Abstract

This research focuses on the inversion of geomagnetic variation field measurements to obtain the source currents in the ionosphere and magnetosphere, and to determine the geoelectric fields at the Earth's surface. During geomagnetic storms, the geoelectric fields create geomagnetically induced currents (GIC) in power networks. These GIC may disturb the operation of power systems, cause damage to power transformers, and even result in power blackouts. In this model, line currents running east–west along given latitudes are postulated to exist at a certain height above the Earth's surface. This physical arrangement results in the fields on the ground being composed of a zero magnetic east component and a nonzero electric east component. The line current parameters are estimated by inverting Fourier integrals (over wavenumber) of elementary geomagnetic fields using the Levenberg–Marquardt technique. The output parameters of the model are the ionospheric current strength and the geoelectric east component at the Earth's surface. A conductivity profile of the Earth is adapted from a shallow layered-Earth model for one observatory, together with a deep-layer model derived from satellite observations. This profile is used to obtain the ground surface impedance and therefore the reflection coefficient in the integrals. The inputs for the model are a spectrum of the geomagnetic data for 31 May 2013. The output parameters of the model are spectrums of the ionospheric current strength and of the surface geoelectric field. The inverse Fourier transforms of these spectra provide the time variations on the same day. The geoelectric field data can be used as a proxy for GIC in the prediction of GIC for power utilities. The current strength data can assist in the interpretation of upstream solar wind behaviour.

Keywords: Geomagnetic induced currents, Geoelectric fields and currents, Inversion, Modelling

Introduction

Geomagnetically induced currents (GIC) can occur in grounded technical networks, such as electric power transmission grids (Bolduc 2002; Molinski 2002; Kappenman 2003; Pirjola 2005; Pulkkinen et al. 2005; Viljanen et al. 2012), oil and gas pipelines (Pulkkinen et al. 2001; Gummow 2002; Trichtchenko and Boteler 2002), and telecommunication cables and railway circuits (Ptitsyna et al. 2008; Wik et al. 2009; Eroshenko et al. 2010). Solar events, such as geoeffective coronal mass ejections (CME), create disturbances within the Earth's magnetosphere, which can give rise to geomagnetic storms and substorms. During geomagnetic storms, the compression of the magnetosphere by the solar wind, and the interaction of the solar wind with the Earth's geomagnetic field enhance the currents in both the magnetosphere and in the ionosphere (e.g. Bothmer and Daglis 2007). These currents cause fluctuations in the geomagnetic field on the ground. Rapid changes in the geomagnetic field generate geoelectric fields that drive GIC in grounded networks. In power systems, the quasi-DC GIC may saturate transformers. This has the potential of causing the transformers to fail. The consequences may include power blackouts (e.g. Kappenman 2007).

*Correspondence: jdevilliers@sansa.org.za
[1] SANSA Space Science, P.O. Box 32, Hermanus 7200, South Africa
Full list of author information is available at the end of the article

GIC have been found in all grounded conductor networks. Power grids carry electric power from the generators to the general public. In power transmission, the alternating currents must pass through transformers designed to transfer electric power between two or more circuits operating at different voltages. The quasi-DC GIC flowing through a transformer from the phases to the grounded neutral biases the magnetic field in the steel transformer core, effectively offsetting the operating point on its B–H (Albertson 1990; Kappenman and Lu and Liu 1993; Molinski 2002). The transformer can go into half-wave saturation, introducing harmonics to the AC waveform, localised heating, vibration and noise, high reactive power demands, and voltage fluctuations. Such a situation has caused severe damages to the transformers and led to extended blackouts in certain regions, including South Africa, during geomagnetic storms. For further details about GIC impacts on power systems, see Bolduc (2002), Koen and Gaunt (2002), Gaunt and Coetzee (2007), and Kappenman (2007).

There are different means to reduce the GIC risk in power networks. It would be particularly beneficial for power utility operators if a warning system would be available that can predict GIC, after the occurrence of an eruptive event on the Sun. The modelling of GIC in a power system (or any other grounded conductor network) comprises a "geophysical step" and an "engineering step" (e.g. Pirjola 2002). The geophysical step derives the geoelectric field from geomagnetic data and geophysical parameters. The engineering step derives the GIC from the geoelectric field and the power network parameters. We only concentrate on the geophysical step in this paper.

Ionospheric source currents have already been computed before by using the spherical elementary current systems (SECS) method (Amm and Viljanen 1999). The elementary current systems are determined over a grid of surface coordinate positions in a chosen affected region in which a power network resides (see e.g. Pulkkinen et al. 2003; Viljanen et al. 2004; Wik et al. 2008). The SECS method involves setting up a matrix of current elements, fitting a geomagnetic model function, with the currents as linear output parameters, to known geomagnetic measurements at selected observatories in this region, using any decomposition inversion technique.

In this paper, a simplified inversion set-up is used in which ionospheric line currents are computed from geomagnetic field observations on the ground. From these currents, we can estimate the induced geoelectric fields at any location of interest, particularly the geoelectric fields at the Earth's surface responsible for GIC in power grids. For the geoelectric field estimates, the surface impedance is assumed to be uniform over the region spanned by the magnetometers and equal to that which is obtained from the one-dimensional (depth) conductivity profile of a layered-Earth model. We could also utilise the method containing the "piecewise-uniform" assumption about the Earth's conductivity structure (Viljanen et al. 2004; Marti et al. 2014).

The motivation for using the field inversion method to compute ionospheric line currents (De Villiers and Cilliers 2014) lies in using the interaction of solar effects outside of the Earth's magnetosphere, such as the solar wind, with the geomagnetic field. The line current strength can be used as an intermediary parameter for modelling techniques that determine the geomagnetic field at selected locations from the solar wind parameters. This simpler model provides an alternative method to estimate the currents in the ionosphere, which may be more amenable to modelling from upstream inputs for investigating storm characteristics all the way from the Sun to the Earth.

In order to use a realistic conductivity profile for the estimation of the geoelectric field, a new Earth profile was compiled from a shallow (up to 100 km depth) worldwide 3D model (Alekseev et al. 2015) for one location and a deep Earth profile compiled from satellite data (Civet et al. 2015), and they are used in this study. This composite structure is utilised to compute the line currents of the EEJ in the ionosphere from geomagnetic measurements, which are then used to derive the geoelectric field on the ground that drives GIC.

Inversion techniques can be used to determine an appropriate distance in magnetic latitude from the EEJ where the contribution of the EEJ current to the geomagnetic field is negligible. Measured geomagnetic data from two African stations, one away from the EEJ and the other underneath the EEJ, may be used to invert for the strength of the EEJ. Before the inversion is done, a geomagnetic variation due to the EEJ is first isolated from the data. A geomagnetic signature should show up during the daytime indicating that an EEJ is present. From the geomagnetic variation signature, the current strength can be established by inversion.

Background

In this paper, we use an approach that is applied to and based on the general theory for computing the geomagnetic and geoelectric fields at the Earth's surface due to an electrojet or ring current in the magnetosphere above a layered Earth (Häkkinen and Pirjola 1986). The main purpose is to show that the inversion method, successfully used for artificial single frequency data by De Villiers and Cilliers (2014), also works for measured geomagnetic data. In this paper, the inversion method (Eq. 7) is applied to each frequency of the Fourier transform of

the measured geomagnetic data. Here only the strength of the current is determined, while the assumed height of the equatorial electrojet is fixed as 100 km, turning the inversion from a nonlinear into a linear optimisation problem. The origin of the equatorial electrojet position is taken to be at the magnetic dip equator.

We consider a physical set-up, in a Cartesian coordinate system where $x =$ north, $y =$ east, and $z =$ down, consisting of a line current $j(x, \omega) = J(\omega)\delta(x - x_o)$ running east–west at a certain height h above the Earth's surface at a given surface position x_o in kilometres along a geomagnetic meridian from the geomagnetic north pole. The function $\delta(x - x_o)$ is the Dirac delta function and is nonzero only at position x_o where the line current is located. The current strength $J(\omega)$ is complex-valued in the frequency domain and will be determined by inversion methods. The only geoelectric field component that is nonzero is eastward (while the northward and downward components are both zero) $\left[E_y(x, \omega) \neq 0,\ E_x(x, \omega) = E_z(x, \omega) = 0\right]$. The only zero geomagnetic component is also eastward (while the northward and downward components are both nonzero) $\left[B_y(x, \omega) = 0,\ B_x(x, \omega) \neq 0,\ B_z(x, \omega) \neq 0\right]$. This is illustrated in Fig. 1.

Currents are induced within the conducting Earth, and so any electromagnetic fields are partially reflected back into the space (Boteler and Pirjola 1998). This is described by the reflection coefficient expressed as

$$R(\nu, \omega) = \frac{\mathrm{i}\omega\mu_0/\nu - Z(\nu, \omega)}{\mathrm{i}\omega\mu_0/\nu + Z(\nu, \omega)} = \frac{\mathrm{i}\omega\mu_0 - \nu Z(\nu, \omega)}{\mathrm{i}\omega\mu_0 + \nu Z(\nu, \omega)} \quad (1)$$

where μ_0 is the free space permeability, ω is the angular frequency, and ν is the horizontal wavenumber. The surface impedance $Z(\nu, \omega)$ can be calculated from a recursive relation based on the Earth's underlying conductivity model (Wait 1958, 1980).

Let us denote the conductivity, thickness, and permeability of the n'th Earth-layer by σ_n, h_n, and μ_n, respectively. In this paper, μ_n and ε_n are assumed to be equal to permeability μ_0 permittivity ε_0 in a vacuum. A recursive relation for the impedance at the top of layer n is

$$Z_n = K_n \frac{Z_{n+1} - K_n \tanh \gamma_n h_n}{K_n - Z_{n+1} \tanh \gamma_n h_n} \quad (2)$$

where $K_n = \mathrm{i}\omega\mu_n/\gamma_n$ is the characteristic impedance of layer n and $\gamma_n = \sqrt{\nu^2 + \nu_n^2}$ is the propagation constant of layer n (with $\nu_n = \sqrt{\mathrm{i}\omega\mu_n\sigma_n - \omega^2\mu_n\varepsilon_n}$). This leads to a spectrum of the surface impedance estimates for the particular location, namely $Z_1 = Z(\nu, \omega)|[h_n, \sigma_n]$, where the structure dependent parameters $[h_n, \sigma_n]$ range over a finite number of layers of the concuctivity model. The

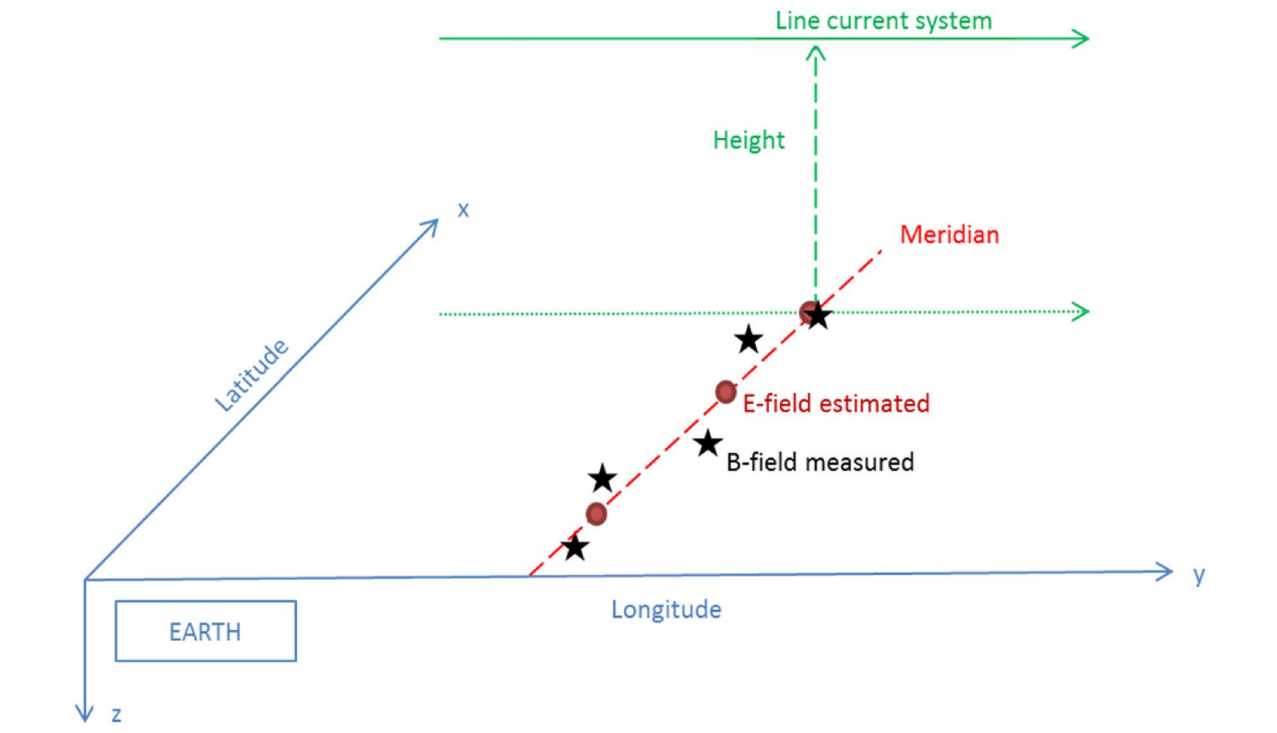

Fig. 1 Physical arrangement. Geomagnetic field measurements and geoelectric field estimations along a meridian with an ionospheric line current system as indicated

complex skin depth is related to the surface impedance by $p(\nu, \omega) = Z(\nu, \omega)/\mathrm{i}\omega\mu_0$.

A diffusion equation for E_y can be derived from Maxwell's equations (Hermance and Peltier 1970), in Cartesian coordinates:

$$\nabla^2 E_y = \mathrm{i}\omega\mu_o\sigma E_y, \tag{3}$$

where $\nabla^2 = \frac{\partial^2}{\partial x^2} + \frac{\partial^2}{\partial z^2}$.

A trial solution, $E_y = \mathrm{e}^{\zeta z}\cos \nu x$, valid for a line current system, is substituted into Eq. (3) to give

$$\left[\frac{\partial^2}{\partial x^2} + \frac{\partial^2}{\partial z^2}\right]\left(\mathrm{e}^{\zeta z}\cos \nu x\right) = \left[-\nu^2 + \zeta^2\right]\left(\mathrm{e}^{\zeta z}\cos \nu x\right) = \mathrm{i}\omega\mu_o\sigma\left(\mathrm{e}^{\zeta z}\cos \nu x\right). \tag{4}$$

Cancelling the trial solution on both sides leads to the relation $\zeta^2 = \nu^2 + \mathrm{i}\omega\mu_o\sigma$. The two roots of this equation would result in both an incident ($\mathrm{e}^{-\zeta z}$) and a reflected ($e^{+\zeta z}$) wave. The solution is symmetrical around $x = 0$ km. Above the Earth's surface ($z < 0$ km), the conductivity of air is assumed to be zero (i.e. $\sigma = 0$ S/m), so $\zeta = \nu$ in this region. Thus, for $z < 0$ km, the geoelectric field elementary solution including the incident ($\mathrm{e}^{-\nu z}$) and reflected ($Re^{\nu z}$) parts with an arbitrary constant C is given by

$$E_y(x, z; \nu, \omega) = C\left[\mathrm{e}^{-\nu z} - R(\nu, \omega)\mathrm{e}^{\nu z}\right]\cos \nu x. \tag{5}$$

One then takes a Fourier integral of the elementary solution over the wavenumber ν. This forms the total geoelectric field at the Earth's surface that depends only on the latitude x and the angular frequency ω (Boteler and Pirjola 1998; Boteler et al. 2000). Through the reflection coefficient $R(\nu, \omega)$, the electric field also depends on the Earth's conductivity profile:

$$E_y(x, \omega) = \mathrm{i}\omega\frac{\mu_0}{2\pi}\int_0^\infty J_\nu(\nu, \omega)\mathrm{e}^{-\nu h}[R(\nu, \omega) - 1]\cos(\nu x)\nu^{-1}\mathrm{d}\nu, \tag{6}$$

where $J_\nu(\nu, \omega) = \int_{-\infty}^{\infty} j(x, \omega)\mathrm{e}^{-\mathrm{i}\nu x}\mathrm{d}x$ is the Fourier transform of the current density for a distribution of currents $j(x, \omega)$ in the real x space. It is possible for this theory to be extended to several line currents or a distribution current over latitude space. However, it introduces additional variables into the model, which may not be uniquely resolvable from the measured data. We will focus only on one line current system. For a line current located at $x_o = 0$: $j(x, \omega) = J(\omega)\delta(x)$, where $J(\omega) = J_\mathrm{r}(\omega) + \mathrm{i}J_\mathrm{i}(\omega)$.

Similar expressions can be derived for the geomagnetic field components on the ground (Boteler et al. 2000), which will be used as the input model functions in the inversion process:

$$\begin{bmatrix} B_x \\ B_z \end{bmatrix}(x, \omega) = \frac{\mu}{2\pi}\int_0^\infty J(\omega)\mathrm{e}^{-\nu h}\begin{bmatrix} \{R(\nu, \omega) + 1\}\cos(\nu x) \\ \{R(\nu, \omega) - 1\}\sin(\nu x) \end{bmatrix}\mathrm{d}\nu. \tag{7}$$

Due to the dependence on $R(\nu, \omega)$ and $J(\omega)$, each of the geomagnetic field components in Eq. (7) is a complex number. In general, the integrals involved in Eqs. (6) and (7) have no analytical solutions (Gradshteyn and Ryzhik 1965) and must thus be solved by some numerical procedure, such as integration by quadrature. Boteler and Pirjola (1998) already derived analytical approximations for the integrals in Eqs. (6) and (7) that are reasonably accurate in many practical situations. Including the derivations here may be beyond the scope of the paper or irrelevant because the approximations that need to be made do not apply to the case we are considering.

The Fourier integrals expressing the ground geomagnetic field components (7) are the model functions in the inversion problem. The input of the inversion of Eq. (7) is the transform of geomagnetic field measurements. The output of the inversion of Eq. (7) is the real $J_\mathrm{r}(\omega)$ and imaginary $J_\mathrm{i}(\omega)$ parts of a line current $J(\omega)$ above the Earth. Once $J(\omega)$ is found, it is substituted into Eq. (6) to estimate the geoelectric field on the ground.

The ionospheric current and the associated surface electric field at the given location and any other location along the meridian, as obtained from the inversion of surface geomagnetic data, are the key contributions of this article.

Methods

Data collection and preparation

Measured geomagnetic data are available at geomagnetic observatories and magnetometer stations around the world. Figure 2 displays a map of the African locations under the EEJ region where geomagnetic data are available as of 2013, including two stations from the INTERMAGNET network (Kerridge 2001) and five from the AMBER network (Yizengaw and Moldwin 2009). Data from both these networks are freely available to any scientist wishing to use them for non-commercial purposes.

Two stations are chosen so that they lie along a given geomagnetic meridian within the region of the EEJ. One of these stations must be approximately underneath the EEJ (we chose Addis Ababa, Ethiopia: 5.32°N Geomagnetic, 0.90°N Apex). Another station must be on the edge of influence of the EEJ (we use Adigrat, Ethiopia: 10.36°N Geomagnetic, 6.84°N Apex). The EEJ is located at the magnetic dip equator (0°N Apex), with a region of influence of only 6–9 degrees of dip latitude on either side. Details of the observatories are given in Fig. 2 and Table 1. It is possible to use data from more than two stations in this set-up, if they are located along the same meridian, and that might improve the inversion results. At present, there exist no magnetometers between Addis Ababa and Adigrat. These two stations are the only ones

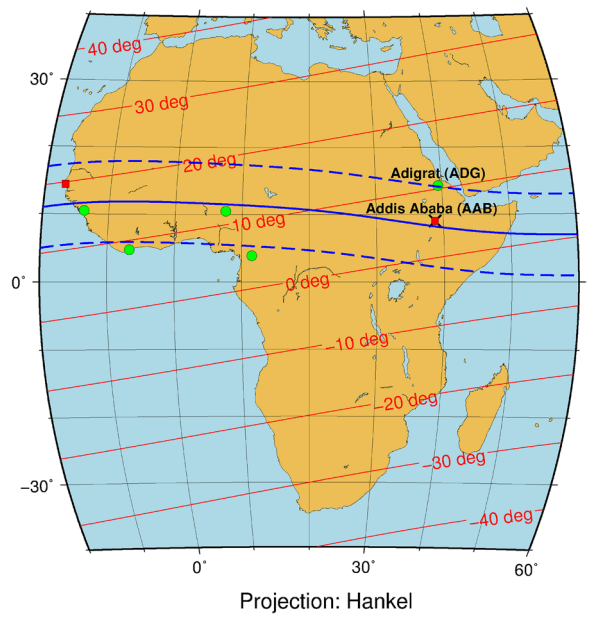

Fig. 2 Map of available African geomagnetic observatories under the influence of the EEJ. Data used in this study are collected only in Ethiopia. The names and coordinates of the two Ethiopian stations are given in Table 2. *Red contours* are geomagnetic latitudes. *Blue curves* show the extent of the EEJ. The *black cross* shows the location of the conductivity profile of Table 1 and Fig. 2 under the closest station. *Symbols* of the other available stations (AMBER: *green circle*, INTERMAGNET: *red square*)

we can work with that are close enough to the geomagnetic equator.

The measurements at these stations are given in either (B_x = north component, B_y = east component, B_z = vertical component) or (B_h = horizontal component, B_d = declination component, B_z = vertical component). If the data are given in the (B_h, B_d, B_z) format, they are converted to the (B_x, B_y, B_z) format. Each station's geomagnetic data are sampled at 1 min intervals.

The EEJ runs along a major part of the geomagnetic equator around the world. However, due to the presence of a South Atlantic Anomaly, the EEJ deviates to the north between about 55°W and 55°E geographic longitude along the magnetic dip equator. This includes Africa, and it complicates the physical set-up of the inversion. Ideally, the inversion should be run over latitude space along a meridian. More accurately, it should be done over the space created along the direction perpendicular to the direction of the EEJ at the given meridian. This is not a true geographic meridian, but deviates a bit to the east. Because the geomagnetic observatories are on different geographic longitudes (as given in Table 1), a meridian position along the EEJ midway between the observatory positions was chosen: 39.115°E. We found the geographic latitude of the EEJ at this longitude to be around 8.17°N for Apex(epoch 2013.5) and 8.15°N for IGRF(epoch 2013), by virtue of the fact that the geomagnetic vertical component and inclination must be zero ($B_z = 0$ nT; $B_I = 0°$) at the EEJ.

Now, we find the geomagnetic declination B_d where the EEJ crosses this meridian and the direction perpendicular to B_x is the direction of the EEJ. The declination is $B_d = 1.85°$ (Apex) and 1.89° (IGRF) east of north. Likewise, the horizontal component is B_h = 35,499.24 nT (Apex) and B_h = 35,395.7 nT (IGRF). The north component is found to be B_x = 35,480.73 nT (Apex) and B_x = 35,376.4 nT (IGRF). The difference $B_h - B_x$ is 18.51 nT (Apex) and 19.3 nT (IGRF), leading to an error percentage of 0.0521 % (Apex) and 0.0545 % (IGRF) with respect to B_h and B_x. It is thus justified to simplify using the geographic coordinate system by showing that the error incurred by not doing the inversion along the direction B_d of B_h would not be significant. We keep the geomagnetic latitudes for illustrative reference in Fig. 2.

The date 31 May 2013 was chosen because Adigrat has the most complete data, with only four gaps, on this storm than on any other storm during its operational lifetime. AMBER's magnetometer at Adigrat began recordings in 2012. Its measurements have constantly been interrupted for unknown reasons in its entire operation. By 30 September 2013, the recordings stopped and were never resumed. By contrast, the magnetometer at Addis Ababa continues to record without a hitch practically since INTERMAGNET started operating.

Table 1 Locations of the African stations where geomagnetic data are collected for this study

Observatory	Coordinates [zero altitude assumed]			Network
	Geographic	Geomagnetic[a] (IGRF 2013)	Apex[b] (Year 2013.5)	
Addis Ababa, Ethiopia	9.03N, 38.77E	5.32N, 112.37E	[0.9018N; 0.9022N], 111.90E	INTERMAGNET (AAE)
Adigrat, Ethiopia	14.28N, 39.46E	10.36N, 113.89E	[6.8432N; 6.8469N], 112.36E	AMBER (ADET)

The stations belong to two different networks

[a] From http://wdc.kugi.kyoto-u.ac.jp/igrf/gggm/index.html

[b] From http://ccmc.gsfc.nasa.gov/coord_transform/index.php; Source (Richmond 1995); Apex format [MagApex-Latitude; QuasiDipole-Latitude], MA/QD-Longitude

There may be a number of reasons for the lack of data (among others, useless recordings, equipment malfunction, faulty or no calibrations, human maintenance and other interventions, as well as power failures), but there are also techniques for overcoming them. This may include data interpolation, or replacement of appropriate data from other neighbouring stations and from past observations. In this paper, linear interpolation is imposed to connect the last available datum with the next available datum over each intervening gap, provided the gaps are not too large ($\leq$1 h) and there is more than half a day's worth of data available for any chosen day.

Then, the geomagnetic variation due to the EEJ is determined at each location by subtracting the midnight component values at the start of the day and the solar quiet (Sq) variations during the day (McPherron 1998; Wanliss and Showalter 2006), which contains the diurnal variation around midday. Before subtraction, the Sq variations were obtained by averaging over ten quiet days during the same month of the period of interest. The Sq is then removed at all local times of the chosen day. The final variations are then ΔB_x and ΔB_z, and they give an indication of the EEJ current. Figure 3 shows what these data from Addis Ababa and Adigrat look like.

Taking Fourier transforms

Because the physical calculations and the inversion are carried out in the frequency domain, the fast Fourier transform (FFT) is taken of the differences ΔB_x and ΔB_z over the given time frame of the chosen day: $T = N\Delta t = 24\,\text{h} = 1440\,\text{min}$. Because the data are sampled at 1-minute intervals, we have a constant time increment $\Delta t = 1\,\text{min} = 60$ s (with the number of samples $N = 1440$ for the given period), $t = \Delta t[(j-1)/N]$ where j is the index over time.

The FFT is similarly discretised with the same number of sampled points (N) in the frequency domain. The k'th spectral component $\mathcal{F}_k = \frac{1}{N}\sum_{j=1}^{N} \varepsilon^{(j-1)(k-1)} F_j$, where $\varepsilon = \mathrm{e}^{-2\pi\mathrm{i}/N}$ is the complex root of unity, is complex-valued and takes on the units of real-valued F_j data. In this application, the physical unit for the geomagnetic field spectra is nanotesla (nT). Thus, $\mathcal{F}_k$ contains amplitude and phase information of the differences ΔB_x and ΔB_z at frequency $f = \Delta f[(k-1)/N]$, where $\Delta f = \frac{1}{\Delta t} = 16.67$ mHz is the sampling frequency.

The brickwall low-pass filter is then applied in which all amplitudes above a certain cut-off frequency are suppressed. The cut-off frequency f_c was chosen to be one-eighth of one-half of the sampling frequency (i.e. the Nyquist frequency f_{Nyquist}). The individual and cumulative spectra shown in Fig. 3 include this filtering.

To check that no essential data were lost (except for smoothing) when the filter was applied, the inverse Fourier transform of the resulting spectra were plotted below the measurements in Fig. 3. We shifted this smoothed curve downwards so that it is not obscured by the actual measurements. The shift was taken as 20 % of the geomagnetic range (the maximum minus the minimum of the given data set) of each component.

Layered Earth and surface impedance

The Earth conductivity profile for Addis Ababa, Ethiopia (the closest magnetic observatory to the EEJ), was compiled from a conductivity model on a three-dimensional grid of the entire world and up to 100 km deep (Alekseev et al. 2015). The deep-layer conductivity profile was derived from geomagnetic measurements obtained by the Swarm satellite (Civet et al. 2015). Table 2 and Fig. 4 present the conductivity profiles combined.

The surface impedance was calculated from this combined layered-Earth model. This is shown as a plot of the surface impedance against angular frequency in Fig. 5. The conductivity profile at the particular location has an impact on the geomagnetic field, which creates a reflection of electromagnetic waves from the Earth's surface and from layer boundaries below the surface.

Frequency properties of the surface impedance

In Fig. 5, one can see that the real and imaginary parts of the surface impedance $Z(\omega)$ are not equal, even though they do not differ very much. In the log–log scale representation, the impedance components have a nonlinear relation to the frequency. The source of this behaviour is the hyperbolic tangent function, $\tanh \gamma_n h_n$, in the recursive relation (2).

On the other hand, the characteristic impedances K_n of the layers are also present in relation (2) and must always be proportional to the square root of the frequency, in the quasi-static approximation (Rikitake 1951), within each layer n. The real and imaginary parts of K_n are equal, which gives a linear plot on the log–log scale.

Further analyses of the frequency dependence of the surface impedance of a layered-Earth model are beyond the scope of this article.

Inversion for finding the current strength parameters

We pick one frequency in the spectrum and collect the corresponding complex Fourier transforms of the differences $\Delta B_x(x, t)$ and $\Delta B_z(x, t)$. An inversion process is run, with input data $\Delta B_x(x, \omega)$ and $\Delta B_z(x, \omega)$ at the selected frequency, using the Levenberg–Marquardt (LM) technique (Lourakis 2005). Simpler alternatives, like the decomposition techniques, can also be used in this linear inversion set-up. However, we keep a general model formulation so that we may easily accommodate the nonlinear parameters of the current system in the future. In this way, we

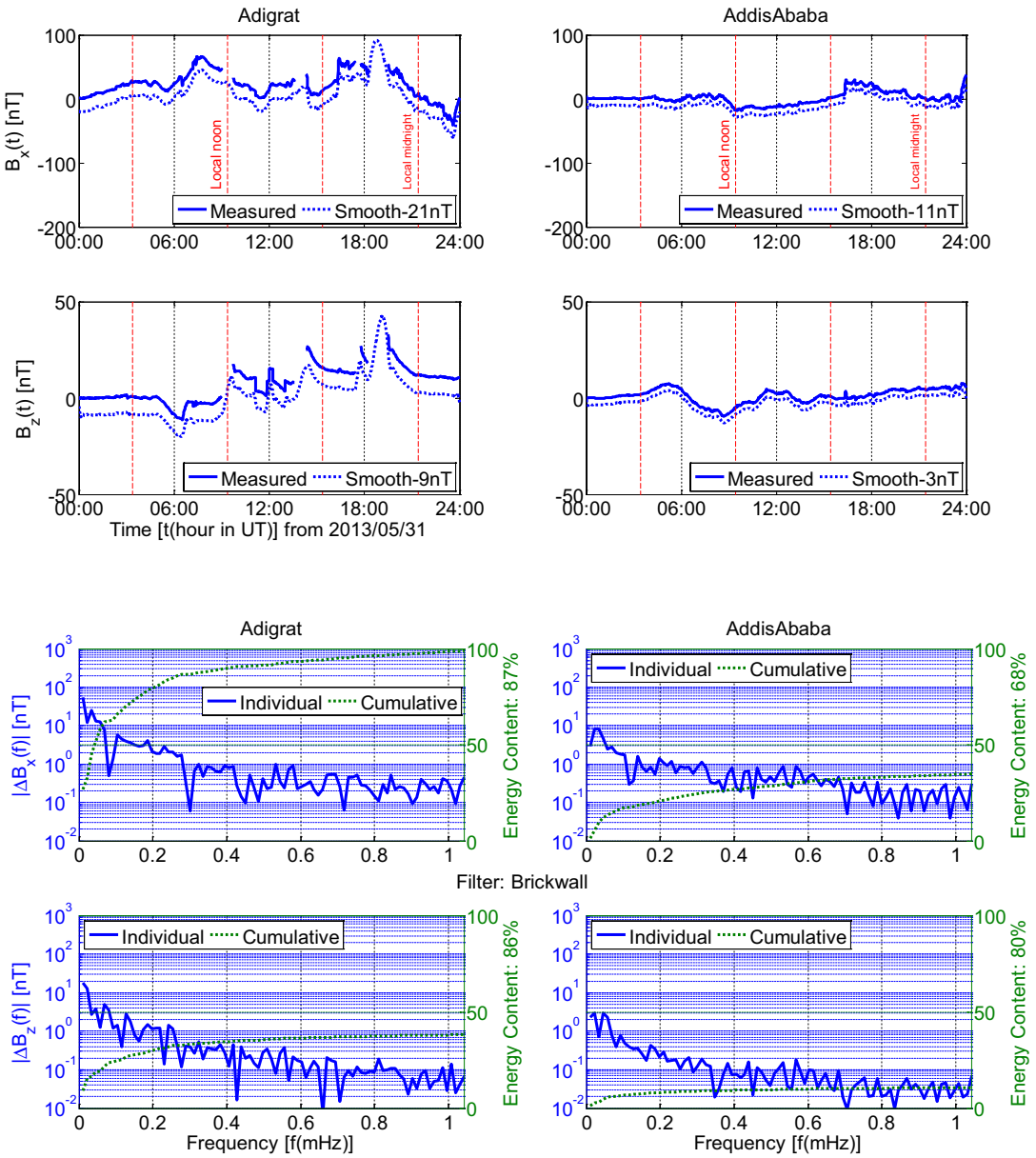

Fig. 3 Geomagnetic ΔB_x (*north*) and ΔB_z (*vertical*) components from Addis Ababa and Adigrat. On 31 May 2013 there is a sudden commencement occurring at 16:19 UT starting a geomagnetic storm. The individual (*left axes*) and cumulative (*right axes*) Fourier spectra of the filtered data are presented in the last *four panels*. Also shown is the percentage of total energy content for each component and station, filtered below the cut-off frequency $f_c = f_{\text{Nyquist}}/8 = 1.04$ mHz (or period: 16 min)

remain consistent with De Villiers and Cilliers (2014). The objective function is a sum-of-squares of residuals that contain Eq. (7) as the model function with model output parameters. The current strength is in the space-frequency domain; its position is the line current system position [i.e. $x = x_o = 0$ as determined from $\delta(x)$]. The complex current strength $J(\omega)$ is estimated as two output parameters [$J_r(\omega)$ and $J_i(\omega)$] in this study. Because the LM technique cannot work with complex numbers, the real and imaginary parts of $J(\omega)$, $\Delta B_x(x, \omega)$ and $\Delta B_z(x, \omega)$, are treated separately. The inversion runs by fitting the model function to the data by optimisation of the model parameters. Once fitted the final values of the parameters constitute the solution to the inversion problem. Figure 6 gives

Table 2 Parameters of a combined 1D model of the ground conductivity structure

Layers	Depth (km)	Conductivity (mS/m)	Place
Layer 1	0.1	20.00	Addis Ababa, Ethiopia
Layer 2	8.0	0.02	
Layer 3	31.0	5.00	
Layer 4	100.0	10.00	
Layer 5	600.0	1.0	Global (Swarm)
Layer 6	900.0	5.2	
Layer 7	1250.0	2700	
Layer 8	∞	3750	

The model is based on magnetotelluric measurements (adapted from Alekseev et al. 2015 to four layers) and satellite measurements (adapted from Civet et al. 2015 to four layers)

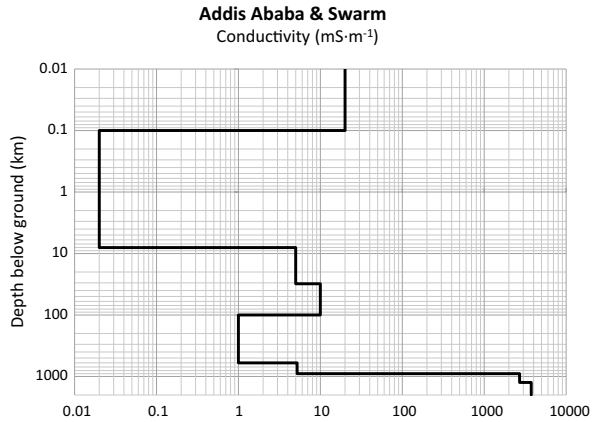

Fig. 4 1D model of the ground conductivity structure used in this study. This structure is obtained from the combination of the data given in Table 1

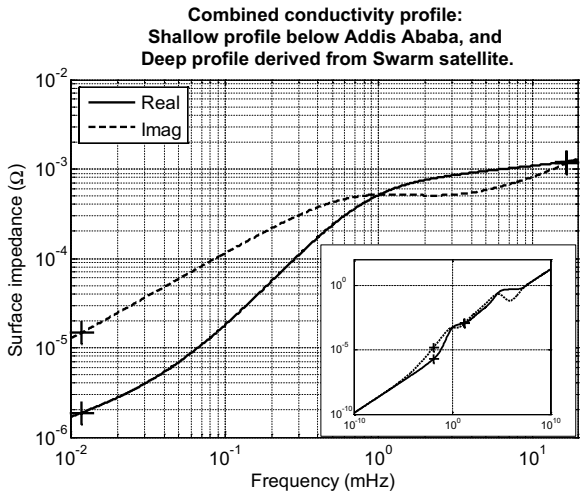

Fig. 5 Surface impedance $Z(\nu = 0, \omega)$ calculated using the layered-Earth model presented in Table 2 and Fig. 2. Crosses are the lowest and highest possible sampled frequencies created by the fast Fourier transform of 1-min geomagnetic data collected on 31 May 2013. Inserted is the same plot at a larger frequency range showing linear behaviours at both ends representing the *bottom* (low frequency) and *top* (high frequency) layers of the conductivity profile. All the linear behaviours of the middle layers are hidden by the nonlinear behaviour of the tangent function, compounded recursively at every iteration of Eq. (2)

the inversion of the geomagnetic components against latitude for one frequency [the last sampled frequency at cut-off: $f_0 = 1/(16\,\text{min} * 60\,\text{s/min}) \simeq 1.04$ mHz]. The resulting fit residuals can be used as a quantitative proxy for the reliability of the model and results. The inversion technique is considered to have converged when the change in the relative function is less than the tolerance. See Tarantola (2005) and Chave and Jones (2012) for a more comprehensive description of the inversion theory and MathWorks Inc. (2015) for the LM tool used.

The inversion is repeated for every frequency of the spectrum that was used for the geomagnetic data. Thus, a spectrum of corresponding modelled geomagnetic values is set up in the frequency domain. An inverse FFT is taken to convert to the real-valued modelled geomagnetic variations in the time domain. Figure 7 shows the spectrum of modelled variations and its inverse Fourier transform. For comparison, the figure also shows the measured variations in both domains.

Current strength and electric field calculation

This repetition of the inversion at every frequency also results in a complex-valued spectrum for the current strength from which an inverse FFT is taken to convert to the real-valued current variations $J(t)$ in the time domain. Figure 8 shows the spectrum of J and its inverse Fourier transform. Once this spectrum is obtained, it can be substituted into Eq. (6) and the spectrum of the eastward component of the geoelectric field at the Earth's surface can be calculated for any location x assuming that the Earth's conductivity profile affecting the reflection coefficient R is known. This spectrum is also converted to the time domain $E_y(x, t)$ by inverse FFT. Figure 9 shows the spectrum of E_y and its inverse Fourier transform. In Figs. 8 and 9, the time domain is the same as that of the measured geomagnetic data. The high peaks at both midnights in Figs. 7, 8 and 9 are the result of a Gibbs phenomenon in the inverse Fourier transform due to a jump discontinuity in the spectrum.

Results

The results of the inversion are depicted in Fig. 6 in terms of $\Delta B_x(x, \omega)$ and $\Delta B_z(x, \omega)$, the measured data at Adigrat

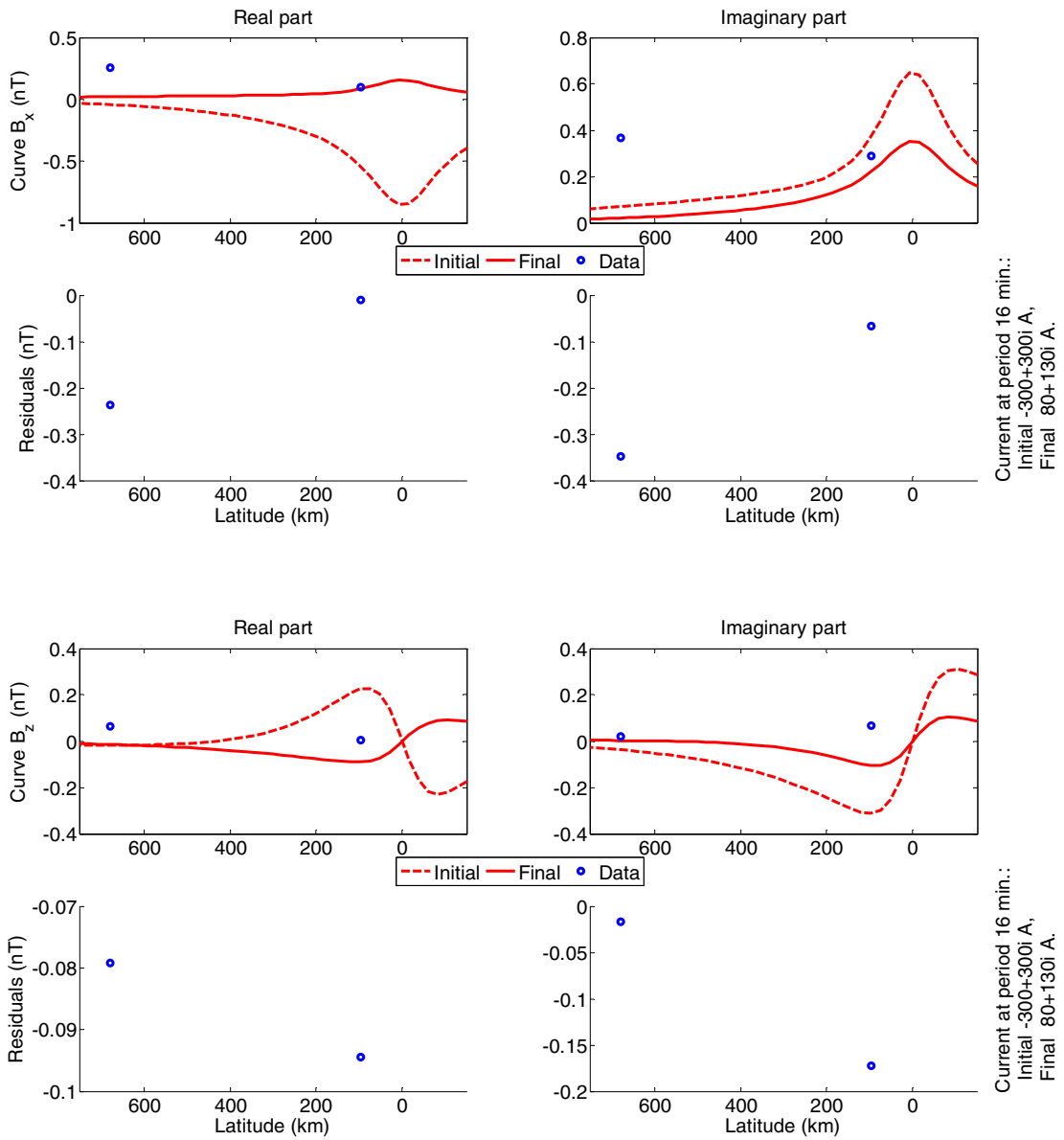

Fig. 6 Inversion from geomagnetic measurements at cut-off 1.04 mHz to determine the parameters of ionospheric currents. "Initial" in the legend refers to the initial estimate to start the inversion. "Final" refers to the inversion result for the same parameter at this cut-off frequency. The residuals (*bottom plots*) are the difference between the inversion results and the measured values (*upper plots*: *circles*) at the locations of Adigrat [678.6 km] and Addis Ababa [95.8 km north of the EEJ] along the geographic meridian

and Addis Ababa. This figure is shown as an example for only one sampled frequency (f_0) of the spectrum of the Fourier transform of $\Delta B_x(x, \omega)$ and $\Delta B_z(x, \omega)$. If the inversion is repeatedly run using data from all sampled frequencies, the performance is similar to Fig. 6.

It is possible that the results will improve if more than two stations were used in the inversion set-up. However, we suspect that the residuals of magnetometers will increase as one goes further away from the ionospheric current system, based on what we have observed with the two magnetometers we considered. Comparing the stations, the data points of Adigrat are far from the inversion result and therefore the corresponding residuals are relatively large, while the data points at Addis Ababa are closer to the inversion (with small residuals). Therefore, the inversion at Addis Ababa can reflect the geomagnetic field more accurately. Being nearly underneath the EEJ, this accuracy at Addis Ababa transfers to the estimation

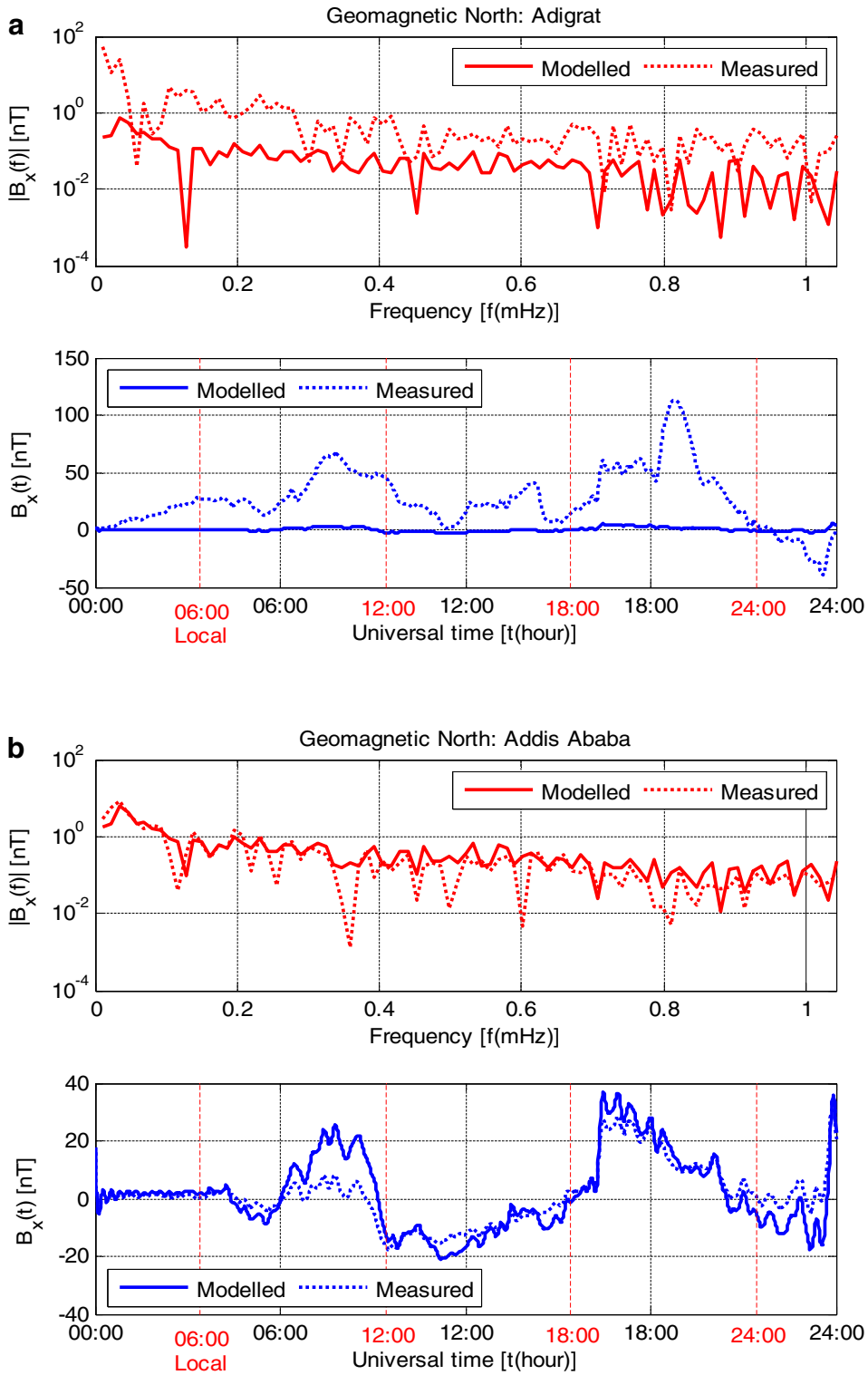

Fig. 7 North component of the geomagnetic field on 31 May 2013. The spectrum (*upper panel*: *solid*) of the geomagnetic field at the surface of the Earth was determined from the Fourier integral of the equatorial electrojet. The time series of the geomagnetic field (*lower panel*: *solid*) was obtained by an inverse Fourier transform of the spectrum. The measured data from Fig. 4 (*both panels*: *dotted*) is also shown. Location: **a** Adigrat, **b** Addis Ababa

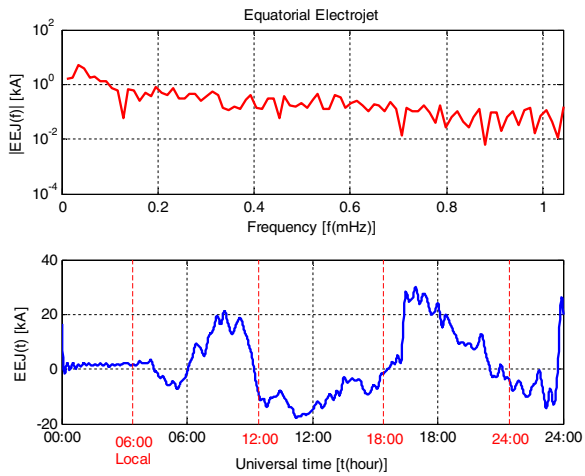

Fig. 8 Equatorial electrojet current strength and its spectrum for 31 May 2013. The spectrum (*upper panel*) was derived from the inversion. The electrojet (*lower panel*) is obtained by an inverse Fourier transform of the spectrum

of the electric field (Fig. 8) and in that of the current strength (Fig. 9) as well.

The line current model is a simplified first approximation used in this paper to show that the developed inversion procedure works for real geomagnetic variation data. It is beyond the scope of this paper to determine a better model. Addis Ababa is 0.9° (in Apex latitude) north of the mean location of the EEJ, but the exact location of the EEJ during this particular storm is not known.

The poor fit in Adigrat could be the result of a Sq current contribution that was not adequately removed from the magnetic data. We tried to remove any Sq current contributions from magnetometer measurements and model only for the EEJ currents. However, the Sq may still contribute to the large residual at Adigrat (and a small part resulting in a small residual at Addis Ababa). Despite these challenges, the fit residual can be used as a quantitative indicator of the reliability of the model and results.

Figure 7 shows a comparison of modelled and measured data of ΔB_x at Addis Ababa for all frequencies of the spectrum. With a few exceptions, the modelled data closely follows that of the measured data. The exceptions are that at some isolated frequencies the spectra of the measurements are much lower than the corresponding modelled spectra. These dips were invisible to the inversion process at those particular frequencies. As a result, the corresponding modelled time series are slightly higher than the corresponding measured time series during most of the day. However, by adding the mean diurnal Sq variation and the midnight value at the start of the day to both time series data, this difference between the modelled and measured variation in the EEJ geomagnetic signature is less pronounced and could be neglected. This step creates the modelled total values of B_x and restores the original absolute measurements from which they were subtracted in the first place.

An excellent correlation between the measured time series of ΔB_x in Fig. 7 and the modelled time series of the EEJ in Fig. 9 is found. A simple linear regression of the relationship determines that a unit change in nanotesla (nT) of ΔB_x corresponds to a large change in the EEJ current strength and small southward geomagnetic offset still exists when the current changes direction. The good correlation (+88.18 %) confirms the adequacy of the method for estimating the EEJ and provides a useful scaling factor [slope 970 Amperes/nanotesla (A/nT); offset 172 nT at 0 A] to relate changes in the geomagnetic field to corresponding changes in the EEJ. Positive and negative values of ΔB_x indicate the EEJ is eastward and westward, respectively. From Fig. 7, it can be seen that the EEJ was first eastwards before local noon and then westwards after local noon in Ethiopia. Also notable is the presence of a sudden commencement in the current strength (from 2.29 to 28.35 kA) later in the day of interest, 31 May 2013, corresponding to a geomagnetic signature (from 4.59 to 27.42 nT).

Discussions

Wider implications for the surface impedance

The frequency range of Fig. 5 was extended to its asymptotic extremes and included as an insert to this plot. In the insert plot, the asymptotes of $Z(\omega)$ at frequency extremes are linear on a log–log scale. At the high frequency end (small skin depth), $Z(\omega)$ approaches the surface impedance of a homogeneous Earth with conductivity equal to that of the top layer [i.e. the short-wavelength (see appendix) EM-waves dominate in the first surface layer of the conductivity profile]. At the low frequency end (large skin depth), $Z(\omega)$ approaches the surface impedance of a homogeneous Earth with conductivity equal to that of the infinite bottom layer [i.e. the long-wavelength EM-waves dominate in the last half-space layer of the conductivity profile]. This asymptotic behaviour is useful for estimating the detail that is required for the conductivity profile if the geoelectric field has to be determined for different rates-of-change of the geomagnetic field.

The geoelectric field

The geoelectric field, at any given position on the ground, is calculated from Eq. (6) with the substituted output parameters (in this case the current strength) obtained after the inversion. If any geoelectric field measurements are available, for example from magnetotelluric studies, the modelled geoelectric field can be tested to determine

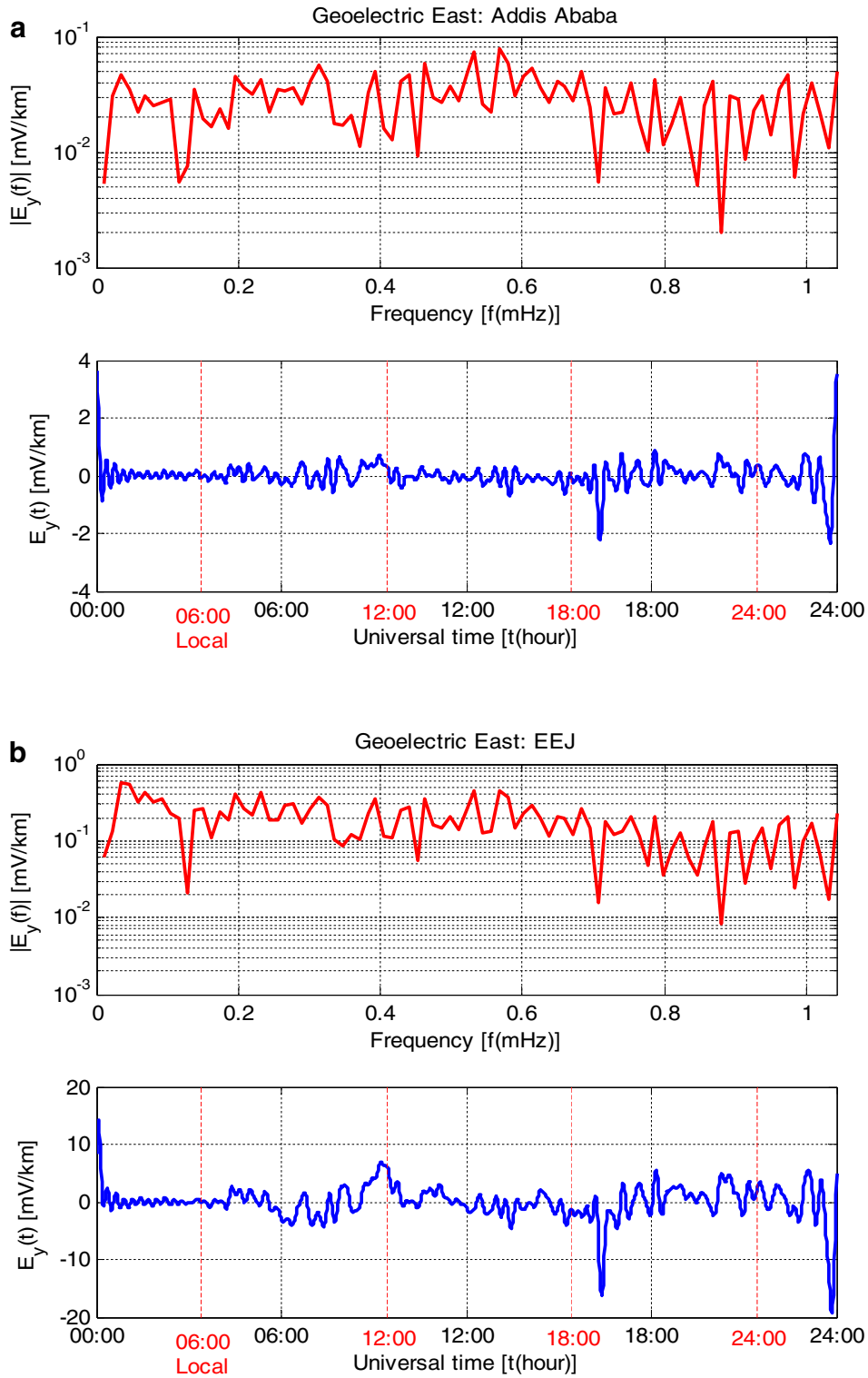

Fig. 9 East component of the geoelectric field on 31 May 2013. The spectrum (*upper panel*) of the geoelectric field at the surface of the Earth was determined from the Fourier integral of the equatorial electrojet. The time series of the geoelectric field (*lower panel*) was obtained by an inverse Fourier transform of the spectrum. Location: **a** Addis Ababa, **b** the EEJ

whether the model functions and its parameters are correct.

The geoelectric field, once computed, also provides a way for GIC in a power network to be predicted, which is of great practical significance. If a suitable model for deriving ionospheric currents during a geomagnetic storms is found from all available data, including several ground-based observations such as the AMIE model (Richmond 1992), then the approach in the present paper could be used to estimate the geoelectric field on the ground and from it estimate the GIC.

When a warning is given in advance, the power utilities can respond in time. Failures in power system operation can then be avoided, and possible transformer damages can be minimised, for example, by rerouting the power to other parts in the grid, or there can be load shedding and the general public can then be warned of a possible blackout more efficiently in advance.

Inversion characteristics

The approach discussed in this paper finds applications in studies of the EEJ. The inversion techniques can be used to determine an appropriate distance in latitude from the EEJ where the effects of the current are no longer seen in the geomagnetic field. Measured geomagnetic data from two stations may be inverted to estimate the strength of the EEJ. A geomagnetic signature should show up during the daytime indicating that an EEJ is present. From this signature, the EEJ current strength can be established by inversion.

There may be a number of factors which affect the performance of the inversion using measured data. In this paper, we used the same inversion method as in De Villiers and Cilliers (2014) that used simulated data at a single frequency to test the inversion. But there are alterations to that inversion method: the distance parameters (height and latitude) is fixed and taken out of the inversion, while the current is now complex-valued. Also in this study actual measured data from Ethiopia were used, and the inversion was done at every frequency in the spectrum of the measured data.

The EEJ is observable only for a few hours around the local noon. For the rest of the day, the electrojet is less pronounced and at night-time it disappears completely. During the day, the EEJ appears and becomes stronger after dawn, peaks near noon, and then weakens towards dusk. However, the sudden commencement and the subsequent geomagnetic storm introduce new dynamic changes to the EEJ, such that the quiet-time variability in subsequent times no longer applies.

The curves of the model function in Fig. 6 may behave non-symmetrically around the EEJ at the Earth's surface, when two different conductivity profiles from each observatory are considered. In this regard, see e.g. Dong et al. (2013) who examine the effects of lateral conductivity variations by putting two different conductivity profiles side-by-side, thus creating a horizontal variation in addition to the vertical variation of conductivities within the ground (cf. Viljanen et al. 2004; Marti et al. 2014). It is possible that such an updated profile to the model function may provide a better fit to the geomagnetic measurements of the two Ethiopian stations.

The geoelectric field has also been used as a proxy for GIC in other studies (e.g. Zheng et al. 2013). Furthermore, Viljanen et al. (2004) and Wik et al. (2008) both take horizontal geomagnetic field data and compute the horizontal geoelectric field directly by multiplication of the surface impedance in a given region. Both went further and computed GIC from the horizontal geoelectric field data on the Swedish and Finnish power networks, respectively. This computed GIC was compared to actual measurements of GIC for a number of storms between the years 1998 and 2000. Viljanen et al. (2004) also used the SECS method to compute equivalent elementary currents and geoelectric fields on a regional grid that spans Finland. In this paper, we only went as far as modelling ionospheric line currents and computing the geoelectric fields from these currents.

Conclusions

The primary contribution from this paper is building on the approach of De Villiers and Cilliers (2014) that used simulated geomagnetic data at one frequency. We applied the inversion method to Fourier transformed data of measured geomagnetic data from Ethiopia. The conductivity profile used in the inversion was derived from a shallow conductivity profile of one Ethiopian station and appended to by a deep Earth conductivity profile determined by the Swarm satellite. The Ethiopian station chosen to construct the conductivity profile was Addis Ababa, which is closest to the EEJ.

The main goal of this paper has been reached, namely that of obtaining time series estimates of the EEJ current strength and of the geoelectric field for 31 May 2013 from geomagnetic measurements. A negative geomagnetic horizontal component difference $\Delta B_x(t)$, just before local noon to local 6 o'clock in the afternoon, indicated a westward current is visible, which implies the presence of a counter electrojet.

A well-defined sudden commencement and subsequent geomagnetic storm is identified at around 16:11 in the inversion modelled data of both the EEJ geomagnetic signature and its current strength. Corresponding to the geomagnetic signature of the sudden commencement, the geoelectric field shows a negative spike (dip) at around the same time. This spike indicates the geoelectric

field is correlated with the time rate-of-change of both the geomagnetic field and EEJ current strength, whereas the current strength itself is strongly correlated with its geomagnetic field.

A time domain approach to the inversion is currently being investigated for its potential to be simpler and faster.

Abbreviations

AC: alternating current; AEJ: auroral electrojet; AMIE: assimilative mapping of ionospheric electrodynamics; AMBER: African Meridian B-field Education and Research (http//magnetometers.bc.edu); CME: coronal mass ejection; DC: direct current; EEJ: equatorial electrojet; FFT: fast Fourier transform; GIC: geomagnetically induced current(s); IAGA: International Association of Geomagnetism and Aeronomy (www.iugg.org/associations/iaga.php); IGRF: International Geomagnetic Reference Field; INTERMAGNET: INTErnational Real-time MAGnetic observatory NETwork (www.intermagnet.org); LM: Levenberg–Marquardt; SECS: spherical elementary current systems; Sq: solar quiet.

Authors' contributions

JSdV conceived of the study, participated in its design and coordination, and drafted and completed the manuscript. RJP and PJC helped to draft the manuscript. All authors read and approved the final manuscript.

Author details

[1] SANSA Space Science, P.O. Box 32, Hermanus 7200, South Africa. [2] Natural Resources Canada, Ottawa, Canada. [3] Finnish Meteorological Institute, Helsinki, Finland. [4] Department of Electrical Engineering, University of Cape Town, Cape Town, South Africa.

Acknowledgements

The authors want to thank the following researchers for the valuable discussion about this research: Donald Danskin (from NRCan), Stefan Lotz (from SANSA), David Oyedokun and Trevor Gaunt (both from UCT). The authors thank E. Yizengaw, E. Zesta, M. B. Moldwin and the rest of the AMBER team for the data from Adigrat. AMBER is operated by Boston College and funded by NASA and AFOSR. The results presented in this paper rely on the data collected at Addis Ababa. We thank Geophysical Observatory of Addis Ababa University and Institut de Physique du Globe de Paris (France), for supporting its operation and INTERMAGNET for promoting high standards of magnetic observatory practice (www.intermagnet.org).

Competing interests

The authors declare that they have no competing interests.

Appendix: Derivation of the spatial wavelength

Usually the symbol λ (lambda) is used for wavelength in tertiary textbooks of the natural sciences, not γ (gamma). From $\nu_n = \sqrt{i\omega\mu_n\sigma_n - \omega^2\mu_n\varepsilon_n}$ defined below Eq. (2), we can identify the $\omega^2\mu_n\varepsilon_n$ term with the classical wavenumber (squared) k_n^2. The wavelength is derived from this wavenumber for layer n: $\lambda_n = \frac{2\pi}{k_n} = 2\pi\left(\frac{c_n}{\omega}\right) = \frac{c_n}{f}$ where $c_n = 1/\sqrt{\mu_n\varepsilon_n}$ is the layer wave speed with f and ω the normal and angular frequency, respectively. The wavelength depends on the speed the wave is travelling through layer n. But because μ_n and ε_n have been set to their corresponding values in free space [see text above Eq. (2)], this speed is everywhere the same; thus $c_n = c$, the speed of light for all layers and also above ground. Therefore, $\lambda = \frac{c}{f}$ and the frequency domain of the spectrum plots in Fig. 3 and elsewhere can be converted to the wavelength domain via this relation.

Received: 12 September 2015 Accepted: 27 August 2016
Published online: 09 September 2016

References

Alekseev D, Kuvshinov A, Palshin N (2015) Compilation of 3D global conductivity model of the Earth for space weather applications. Earth Planets Space 67:108. doi:10.1186/s40623-015-0272-5

Amm O, Viljanen A (1999) Ionospheric disturbance magnetic field continuation from the ground to the ionosphere using spherical elementary current systems. Earth Planets Space 51(6):431–440

Bolduc L (2002) GIC observations and studies in the Hydro-Québec power system. J Atmos Solar Terr Phys 64(16):1793–1802

Boteler DH, Pirjola RJ (1998) The complex-image method for calculating the electric and magnetic fields produced at the surface of the Earth by the auroral electrojet. Geophys J Int 132:31–40

Boteler DH, Pirjola RJ, Trichtchenko L (2000) On calculating the electrical and magnetic fields produced in technological systems at the Earth's surface by a "wide" electrojet. J Atmos Solar Terr Phys 62:1311–1315

Bothmer V, Daglis IA (eds) (2007) Space weather—physics and effects. Springer, Praxis Publ Ltd, Chichester

Chave AD, Jones AG (2012) The magnetotelluric method: theory and practice. Cambridge University Press, Cambridge

Civet F, Thébault E, Verhoeven O, Langlais B, Saturnino D (2015) Electrical conductivity of the Earth's mantle from the first Swarm magnetic field measurements. Geophys Res Lett. doi:10.1002/2015GL063397

De Villiers JS, Cilliers PJ (2014) Applying inversion techniques to derive source currents and geoelectric fields for geomagnetically induced current calculations. Ann Geophys 32:1263–1275. doi:10.5194/angeo-32-1263-2014

Dong B, Danskin DW, Pirjola RJ, Boteler DH, Wang ZZ (2013) Evaluating the applicability of the finite element method for modelling of geoelectric fields. Ann Geophys 31:1689–1698. doi:10.5194/angeo-31-1689-2013

Eroshenko EA, Belov AV, Boteler D, Gaidash SP, Lobkov SL, Pirjola R, Trichtchenko L (2010) Effects of strong geomagnetic storms on Northern railways in Russia. Adv Space Res 46:1102–1110

Gaunt CT, Coetzee G (2007) Transformer failures in regions incorrectly considered to have low GIC-risk. In: Proc. IEEE powertech conference, Lausanne

Gradshteyn IS, Ryzhik IM (1965) Table of integrals, series and products. Academic Press, New York

Gummow RA (2002) GIC effects on pipeline corrosion and corrosion-control systems. J Atmos Solar Terr Phys 64(16):1755–1764

Häkkinen L, Pirjola R (1986) Calculation of electric and magnetic fields due to an electrojet current system above a layered Earth. Geophysica 22(1–2):31–44

Hermance JF, Peltier WR (1970) Magnetotelluric fields of a line current. J Geophys Res 75:3351–3356

Kappenman JG (2003) Storm sudden commencement events and the associated geomagnetically induced current risks to ground-based systems at low-latitude and midlatitude locations. Space Weather 1(3):1016. doi:10.1029/2003SW000009

Kappenman JG (2007) Geomagnetic disturbances and impacts upon power system operation. In: Grigsby LL (ed) The electric power engineering handbook, Chap 16, 2nd edn. CRC Press/IEEE Press, pp 16–22

Kappenman JG, Albertson VD (1990) Bracing for the geomagnetic storms. IEEE Spectr Mag 27(3):27–33

Kerridge D (2001) INTERMAGNET: Worldwide near-real-time geomagnetic observatory data. In: Proceedings of the workshop on space weather, ESTEC, 34. www.intermagnet.org/publications/IM_ESTEC.pdf. Accessed 7 July 2014

Koen J, Gaunt CT (2002) Geomagnetically induced currents at mid-latitudes. In: International Union Radio Science (URSI) General Assembly, Maastricht

Lourakis MIA (2005) A brief description of the Levenberg–Marquardt algorithm implemented by Levmar. Institute of Computer Science, Foundation Research Technology, Hellas

Lu S, Liu Y (1993) FEM analysis of dc saturation to assess transformer susceptibility to geomagnetically induced currents. IEEE Trans Power Deliv 8(3):1367–1376

Marti L, Yiu C, Rezaei-Zare A, Boteler D (2014) Simulation of geomagnetically induced currents with piecewise layered-earth models. IEEE Trans Power Deliv 29(4):1886–1893

MathWorks Inc. (2015) Optimization theory overview. http://www.mathworks.com/help/optim/ug/optimization-theory-overview.html. Accessed 12 March 2015

McPherron B (1998). In: GEM 1998 workshop (slides 18–29) http://slideplayer.com/slide/4307987/. Accessed 25 April 2016

Molinski TS (2002) Why utilities respect geomagnetically induced currents. J Atmos Solar Terr Phys 64(16):1765–1778

Pirjola R (2002) Review on the calculation of surface electric and magnetic fields and of geomagnetically induced currents in ground-based technological systems. Surv Geophys 23(1):71–90

Pirjola R (2005) Effects of space weather on high-latitude ground systems. Adv Space Res 36:2231–2240. doi:10.1016/j.asr.2003.04.074

Ptitsyna NG, Kasinskii VV, Villoresi G, Lyahov NN, Dorman LI, Iucci N (2008) Geomagnetic effects on mid-latitude railways: a statistical study of anomalies in the operation of signaling and train control equipment on the East-Siberian Railway. Adv Space Res 42:1510–1514

Pulkkinen A, Pirjola R, Boteler D, Viljanen A, Yegorov I (2001) Modelling of space weather effects on pipelines. J Appl Geophys 48:233–256

Pulkkinen A, Amm O, Viljanen A, BEAR Working Group (2003) Ionospheric equivalent current distributions determined with the method of spherical elementary current systems. J Geophys Res 108(A2):1053. doi:10.1029/2001JA005085

Pulkkinen A, Lindahl S, Viljanen A, Pirjola R (2005) Geomagnetic storm of 29–31 October 2003: geomagnetically induced currents and their relation to problems in the Swedish high-voltage power transmission system. Space Weather 3(8):S08C03. doi:10.1029/2004SW000123

Richmond AD (1992) Assimilative mapping of ionospheric electrodynamics. Adv Space Res 12(6):59–68

Richmond AD (1995) Ionospheric electrodynamics using magnetic Apex coordinates. J Geomagn Geoelectr 47:191–212

Rikitake T (1951) Changes in Earth current and their relation to the electrical state of the Earth's current. Bull Earthq Res Inst 29:271–276

Tarantola A (2005) Inverse problem theory. Society of Industrial and Applied Mathematics (SIAM), Philadelphia

Trichtchenko L, Boteler DH (2002) Modelling of geomagnetic induction in pipelines. Ann Geophys 20:1063–1072

Viljanen A, Pulkkinen A, Amm O, Pirjola R, Korja T, BEAR Working Group (2004) Fast computation of the geoelectric field using the method of elementary current systems and planar Earth models. Ann Geophys 22(1):101–113

Viljanen A, Pirjola R, Wik M, Adam A, Pracser E, Sakharov Y, Katkalov J (2012) Continental scale modelling of geomagnetically induced currents. J Space Weather Space Clim 2:A17. doi:10.1051/swsc/2012017

Wait JR (1958) Transmission and reflection of electromagnetic waves in the presence of stratified media. J Res Nat Bur Stand 61(3):205–232

Wait JR (1980) Electromagnetic surface impedance for a layered earth for excitation. Radio Sci 15(1):129–134

Wanliss JA, Showalter KM (2006) High-resolution global storm index: Dst versus SYM-H. J Geophys Res 111:A02202. doi:10.1029/2005JA011034

Wik M, Viljanen A, Pirjola R, Pulkkinen A, Wintoft P, Lundstedt H (2008) Calculation of geomagnetically induced currents in the 400 kV power grid in southern Sweden. Space Weather 6(7):S07005. doi:10.1029/2007SW000343

Wik M, Pirjola R, Lundstedt H, Viljanen A, Wintoft P, Pulkkinen A (2009) Space weather events in July 1982 and October 2003 and the effects of geomagnetically induced currents on Swedish technical systems. Ann Geophys 27:1775–1787

Yizengaw E, Moldwin MB (2009) African Meridian B-field Education and Research (AMBER) Array. Earth Moon Planets 104(1):237–246. doi:10.1007/s11038-008-9287-2

Zheng K, Trichtchenko L, Pirjola R, Liu L-G (2013) Effects of geophysical parameters on GIC illustrated by benchmark network modeling. IEEE Trans Power Deliv 28(2):1183–1191